In situ imaging of LPMO action on plant tissues

Amandine Leroy, Mathieu Fanuel, Camille Alvarado, Hélène Rogniaux, Sacha Grisel, Mireille Haon, Jean-Guy Berrin, Gabriel Paës, Fabienne Guillon

Carbohydrate Polymers 343 (2024) 122465

Contents lists available at ScienceDirect

Carbohydrate Polymers

journal homepage: www.elsevier.com/locate/carbpol

In situ imaging of LPMO action on plant tissues

Amandine Leroy [a,b], Mathieu Fanuel [a,c], Camille Alvarado [a], Hélène Rogniaux [a,c], Sacha Grisel [d,e], Mireille Haon [d,e], Jean-Guy Berrin [d], Gabriel Paës [b,*], Fabienne Guillon [a]

[a] INRAE, UR 1268 BIA, 44316 Nantes, France
[b] INRAE, Université de Reims Champagne Ardenne, FARE, UMR A 614, 51100 Reims, France
[c] INRAE, BIBS Facility, 44316 Nantes, France
[d] INRAE, Aix Marseille Université, Biodiversité et Biotechnologie Fongiques (BBF), 13009 Marseille, France
[e] INRAE, Aix Marseille Université, 3PE platform, 13009 Marseille, France

ARTICLE INFO

Keywords:
Oxidative enzyme
Plant cell wall
Cellulose
MALDI-MS imaging

ABSTRACT

Lytic polysaccharide monooxygenases (LPMOs) are copper-dependent enzymes that oxidatively cleave recalcitrant polysaccharides such as cellulose. Several studies have reported LPMO action in synergy with other carbohydrate-active enzymes (CAZymes) for the degradation of lignocellulosic biomass but direct LPMO action at the plant tissue level remains challenging to investigate. Here, we have developed a MALDI-MS imaging workflow to detect oxidised oligosaccharides released by a cellulose-active LPMO at cellular level on maize tissues. Using this workflow, we imaged LPMO action and gained insight into the spatial variation and relative abundance of oxidised and non-oxidised oligosaccharides. We reveal a targeted action of the LPMO related to the composition and organisation of plant cell walls.

1. Introduction

Lytic polysaccharide monooxygenases (LPMOs) are monocopper enzymes secreted by most lignocellulolytic microorganisms, including filamentous fungi. LPMOs are classified in the CAZy database (www.cazy.org) as auxiliary activity (AA) enzymes within eight different families (AA9-AA11, AA13-AA17). AA9 enzymes, which are only encountered in fungi, are active on cellulose with some members also showing activity on hemicelluloses and/or oligosaccharides (Bennati-Granier et al., 2015; Sagarika et al., 2022; Vandhana et al., 2022). LPMOs cleave polysaccharides by abstracting the H atom of the C_1 and or C_4 carbon, releasing C_1-oxidised aldonic acid and/or C_4 oxidised ketoaldose (Tandrup et al., 2018). Cellulose-active LPMOs can act at the surface of cellulose with a disruption of the chain network (Chemin et al., 2023; Villares et al., 2017), therefore increasing the accessibility and activity of glycoside hydrolases (GHs) by creating new chain ends (Eibinger et al., 2017; Vermaas et al., 2015). To be active, LPMOs require an electron donor and O_2 or H_2O_2 (Frandsen et al., 2020; Munzone et al., 2024). The electron source can be extracellular, provided by a redox partner (e.g. cellobiose dehydrogenase), or molecular reductants present in plant cell walls, such as phenols, flavonoids or lignin (Frommhagen et al., 2017; Westereng et al., 2015).

LPMOs are now commonly used either sequentially with hydrolases or combined in commercial cocktails, to enzymatically deconstruct the highly complex matrix that makes up plant biomass: lignocellulose (Gupta et al., 2016). Several studies have demonstrated the synergistic capacity of AA9 LPMOs with GHs on different pretreated lignocellulosic substrates (Agrawal et al., 2020; Caputo et al., 2023; Chabbert et al., 2017; Grieco et al., 2020; Harris et al., 2010; Long et al., 2020), minimising the enzymatic load for polysaccharide degradation and thus reducing the processing costs (Sagarika et al., 2022). However, variations in the efficiency of the synergy between LPMOs and GHs to enhance the saccharification of lignocellulosic biomass have been observed (Bernardi et al., 2020; Moon et al., 2022; Zhou et al., 2020). Many factors may be involved, including the origin of the LPMO, GH partners, reaction environment, LPMO/cellulase ratio, incubation time, and lignocellulosic biomass properties (Chemin et al., 2023; Tokin et al., 2020).

To our knowledge, only few studies have attempted to analyse the direct action of LPMOs at the cellular scale (Chabbert et al., 2017; Chang

* Corresponding author.
E-mail addresses: amandine.leroy@inrae.fr (A. Leroy), mathieu.fanuel@inrae.fr (M. Fanuel), camille.alvarado@inrae.fr (C. Alvarado), helene.rogniaux@inrae.fr (H. Rogniaux), sacha.grisel@inrae.fr (S. Grisel), mireille.haon@inrae.fr (M. Haon), jean-guy.berrin@inrae.fr (J.-G. Berrin), gabriel.paes@inrae.fr (G. Paës), fabienne.guillon@inrae.fr (F. Guillon).

https://doi.org/10.1016/j.carbpol.2024.122465
Received 23 April 2024; Received in revised form 20 June 2024; Accepted 4 July 2024
Available online 5 July 2024

et al., 2022). This is mainly due to the fact that: i) LPMOs act mostly at the surface of their insoluble substrate (Eibinger et al., 2014; Uchiyama et al., 2022; Villares et al., 2017); ii) the amount of oxidised soluble products released by LPMOs can be quite low compared to the degradation products of GHs; iii) the possible variation in LPMO affinity depends on the physico-chemical composition of the polymer cell walls making up the different plant tissues (Devaux et al., 2018; Leroy et al., 2022).

Over the past decade, matrix-assisted laser desorption/ionization mass spectrometry (MALDI-MS) imaging was successfully applied to plant organ thin sections to map modifications in the chemical structure of cell wall polysaccharides as a function of developmental stage, genotype or to assess enzymatic hydrolysis (Arnaud et al., 2020; Fanuel et al., 2018; Granborg et al., 2023; Leroy et al., 2022; Veličković et al., 2014). Building on this previous work, we hypothesised that MALDI imaging could be used to examine the oxidative degradation of plant cell walls. In this study, MALDI-MS imaging was exploited to investigate the behaviour of LPMOs and their synergism with cellulases, in raw and pretreated maize internode samples. The main challenge was to detect the oxidised oligosaccharides resulting from the action of LPMOs. After overcoming technical challenges, we investigated the in situ action of a cellulose-active LPMO alone and in concert with cellulases. These findings were analysed considering cell types and cell wall properties.

2. Materials and methods

2.1. Plant material

The maize genotype F7025 was grown in INRAE experimental plots in Maugio (South of France) under irrigated conditions and harvested at silage stage. The internodes under the main ear were isolated, dried and cut into 2 cm fragments. The fragments were cut in half lengthways and then soluble components were removed by an 8-h ethanol extraction followed with a 48-h water extraction.

2.2. Hot water pretreatment and sample preparation

Two severities of hot water pretreatment (HWP) were performed on the extracted soluble fragment halves at a constant temperature of 180 °C for 20 min (20-min HWP) or 40 min (40-min HWP), with the same experimental conditions as described by (Leroy et al., 2021). Soluble compounds were removed as described above. For imaging and MALDI-MS imaging approaches, raw and 40-min HWP fragments were embedded in polyethylene glycol (PEG), as described by (Leroy et al., 2022). 80 µm thick cross-sections were prepared using a rotary microtome (HM 360, Microm Microtech, Thermo Scientific, USA). This thickness was found as the best compromise between proper tissue sectioning and a decent MS signal. Successive washes with deionized water were performed to remove PEG from the sections. It is important to note that at this stage of preparation, cell wall polysaccharides are not yet enzymatically hydrolyzed and therefore should not be soluble in the washing medium.

2.3. Enzyme preparation

A solution of commercial cellulases from *Trichoderma reesei*, Celluclast® (Novozymes A/D, Denmark), and of *Pa*LPMO9E, C_1-type LPMO supplied by BBF laboratory (Bennati-Granier et al., 2015), were used for enzymatic hydrolysis. The commercial cellulase cocktail has a cellulase activity, xylanase activity and protein loading of 64 FPU.mL^{-1}, 507 IU.mL^{-1} and 50.7 mg.mL^{-1}, respectively in sodium acetate buffer 10 mM pH 5.2. The enzyme solutions were desalted through an Amicon Ultra Centrifugal filter MWCO 10 kDa (ref. UFC501008).

2.4. Matrix-assisted laser desorption/ionization-mass spectrometry imaging

2.4.1. Preparation and in-situ enzymatic hydrolysis of sections

80 µm thick sections were deposited on indium tin oxide glass slides (ref. 8237001, Bruker, Germany) covered with adhesive carbon tape (ref. AGG3939B, Agar Scientific). The LPMO preparation (*Pa*LPMO9E 10 µM, ascorbate 10 mM, sodium acetate 10 mM pH 5.2) and the Celluclast® preparation (0.35 FPU.mL^{-1}) were deposited by nebulisation using a homemade robot on the cross-section (Veličković et al., 2014). The three enzymatic conditions (Celluclast® alone, *Pa*LPMO9E alone, *Pa*LPMOE9 then Celluclast®) were combined on a single slide. First, 0.3 µL.mm^{-2} of the solution buffer (ascorbate 10 mM, sodium acetate 10 mM pH 5.2) was sprayed onto the "Celluclast® alone section" to compensate for the sodium ion doping experienced by the other sections. Then, 0.3 µL.mm^{-2} of the *Pa*LPMO9E solution was sprayed on both "*Pa*LPMO9E alone section" and "*Pa*LPMO9E then Celluclast® section" (incubation at 30 °C for 6 h + 15 h). Finally, 0.3 µL.mm^{-2} of the Celluclast® solution was sprayed on the "Celluclast® alone section" and "*Pa*LPMO9E then Celluclast® section" (incubation at 30 °C for 15 h).

2.4.2. MALDI matrix deposition

A DMA/DHB matrix composed of 100 mg.mL^{-1} 2,5-dihydroxybenzoic acid (DHB) in 50:50 deionized water/acetonitrile, 2 % N,Ndimethylaniline (DMA) was prepared as described by (Ropartz et al., 2011). A thin layer of the MALDI matrix (85 nL.mm^{-2}) was sprayed using an in-house-designed robot (Veličković et al., 2014).

2.4.3. Acquisition and processing of mass spectrometry images

Laser Desorption/Ionization-Mass Spectrometry (MALDI MS) analyses were acquired with a rapifleX MALDI Tissuetyper MALDI-TOF mass spectrometer (Bruker, Germany) with the same acquisition parameters as described by (Arnaud et al., 2020). Briefly, analyses were run with positive polarity and in reflectron mode. One hundred laser shots were accumulated at 10 kHz to obtain one spectrum over a square raster of 20 µm^2 or 40 µm^2. The species detected correspond to singularly charged sodium adducts from the molecules. Given the symmetry of the tissues (Arnaud et al., 2020) and in order to minimize analysis time and avoid MALDI matrix sublimation in vacuum, analyses were carried out on quarter (or half) sections. Acquired MS images were processed with SCiLS software (2016b version). On an MSI image, the coloration of a pixel corresponds to the intensity of an ion (or group of ions) as measured on the mass spectrum corresponding to that pixel. The intensity measured cannot be directly related to the quantity of a species in the tissue. The intensity scale (Jet) is given on each figure with the minimum and maximum intensities measured on the tissues present in the figure. Spectra were normalized on the total ion current (TIC) in SCiLS. For data processing, the number of points per spectrum was reduced to 10,845 over a mass range of 300 to 1240 *m/z*, corresponding to an *m/z* bin width of 0.087. For the bar charts, the average spectra of each section were used. No other data processing was carried out. The average spectrum corresponds to the mass spectrum whose intensity - after TIC normalization - is averaged over the pixels in the area under consideration.

3. Results

3.1. MALDI-MS imaging optimisation to study LPMO action

The fungal AA9 LPMO from *Podospora anserina* (*Pa*LPMO9E), which carries a family 1 carbohydrate-binding module (CBM1) and acts on cellulose, was selected (Bennati-Granier et al., 2015). Its ability to improve saccharification in combination with Celluclast® was first evaluated on native and hot water pretreated (HWP) maize internodes. This pretreatment was chosen as it induces solubilisation of hemicelluloses and some structural changes of lignin and cellulose while

preserving the tissue organisation (Herbaut et al., 2018; Leroy et al., 2021; Pu et al., 2013). The increase in glucose yield was mainly observed for the sample pretreated with hot water at 180 °C for 40 min (40-min HWP) (Fig. S1). The stimulatory effect of *Pa*LPMO9E was then further investigated at the tissue and cell level on raw and 40-min HWP maize internodes by MALDI-MS imaging.

A MALDI-MS imaging workflow was developed to access oxidised oligosaccharides (Fig. 1). The oxidation products of LPMO9E are oligosaccharides with an *aldonic* acid *form* (i.e., a carboxylic acid function). They are detected with a delta mass of +15.995 or 37.977 Da, as compared to non-oxidised species (Fig. S2). The challenge here was to be able to monitor by MS these oxidised species that i) originate from a tissue that is more or less recalcitrant to degradation, ii) are produced in small quantities, iii) compete for detection by MS with the massively released native species (i.e., non-oxidised species). The key step was to optimize enzyme deposition (amount, ratio between enzymes, incubation time and temperature) while limiting both i) the addition of buffers containing salts that are detrimental for the MS signal, and ii) the volumes deposited on the tissue to avoid delocalization of the released species, which would reduce the achievable spatial resolution. The best results were obtained when LPMO and cellulases were applied sequentially. Once all the parameters were optimized, the workflow allowed the detection of the major soluble products released by the enzymatic reaction on plant tissues with a spatial resolution of 20 µm. After reconstruction, MS images showing the distribution and relative abundance of each chemical species can be generated. Comparison of these MS images with light images of the sections allows correlation between the tissue origin and the released specific oligosaccharides. All the spectra corresponding to the species released by the enzymatic reaction were normalized, allowing their intensities to be compared between the different conditions observed. In addition to the synergistic effects of LPMO and Celluclast®, the action of LPMO alone was studied.

3.2. Imaging the synergism between LPMO and cellulases

To visualise at tissue scale the saccharification boost upon the addition of the LPMO, we generated MS images showing the distribution of the sum of cello-oligosaccharides (COS_{tot}), corresponding to the sum of non-oxidised cello-oligosaccharides (COS) and of oxidised cello-oligosaccharides (COS_{ox}) (Fig. 2A). For each condition, four replicates were performed (Figs. S3–S5). In raw internodes sections incubated with cellulases alone or with prior addition of LPMO, COS_{tot} were mainly detected in the parenchyma under the rind and, to a lesser extent, in the parenchyma surrounding the bundles. According to FASGA staining (Fig. S6), these regions correspond to the weakly lignified cell types. In pretreated internode sections incubated with cellulases alone, the intensity of the coloured pixels was lower than that of the corresponding pixels in the raw sample, indicating that fewer COS_{tot} were detected. The COS_{tot} appeared to be more prominent in the parenchyma under the rind and around vascular bundles. When cellulases were combined with *Pa*LPMO9E, COS_{tot} were detected in these two regions in the raw sections and also in the pith in the pretreated sections. Altered lignification in the pith as a result of the pretreatment, visible by FASGA staining (Fig. S6), appeared to have favoured the release of COS_{tot}.

In contrast to saccharification analysis using the reducing sugar assay (Fig. S1), which only detects COS, MS can detect both COS and COS_{ox}, thus allowing determination of their relative contribution to the total signal and their respective amount in the different experimental conditions (Fig. 2B, C). A significant increase in the amount of COS_{tot} released was observed when the LPMO was applied prior to cellulases with a 5-fold increase in HWP internode sections (Fig. 2C), and a more modest (12 %) increase in raw internode sections (Fig. 2B). COS_{ox} were only detected when the LPMO was added and accounted for 3 % and 11 % of COS_{tot} in raw and pretreated internode sections, respectively. The increase in COS_{tot} released with a significant proportion of COS_{ox}

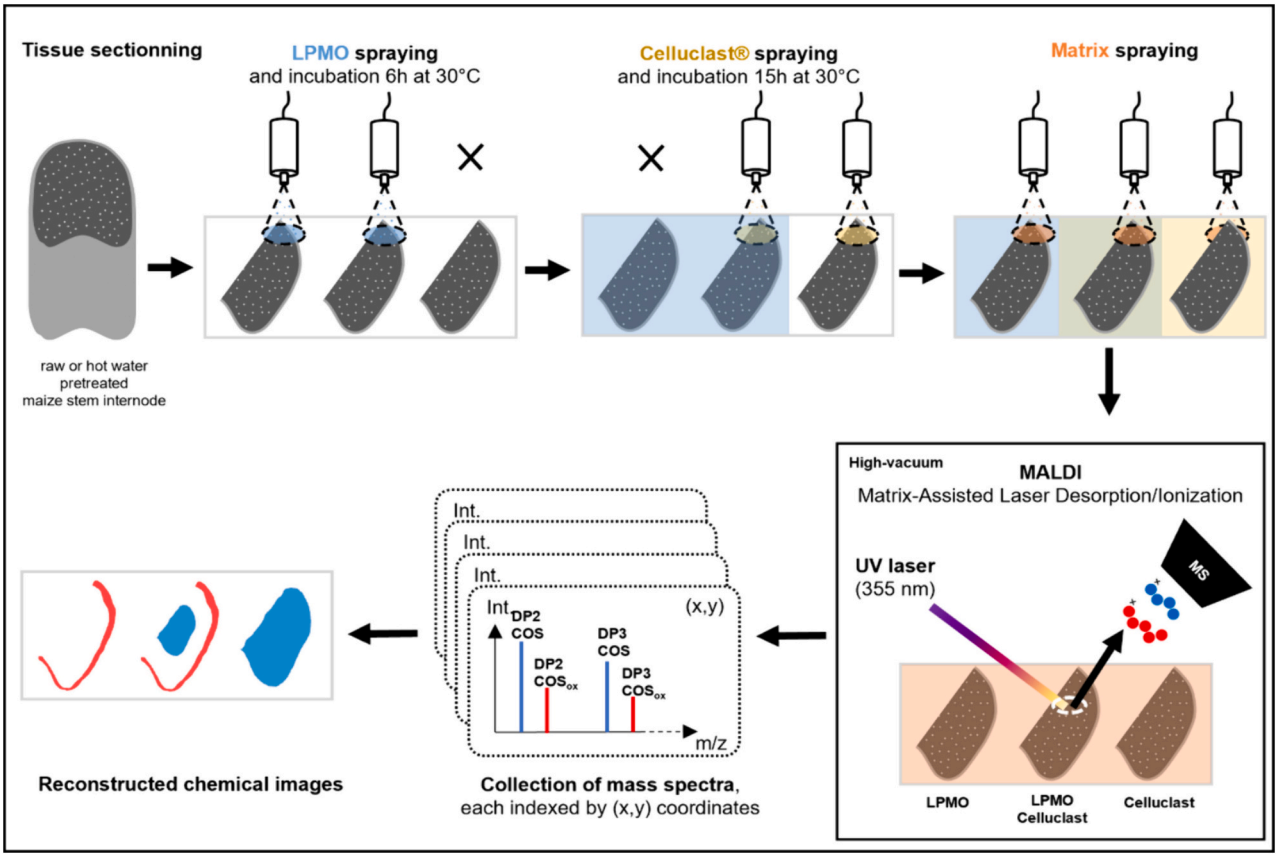

Fig. 1. Schematic representation of the workflow developed for the detection of oxidised cello-oligosaccharides (COS_{ox}) on plant tissues.

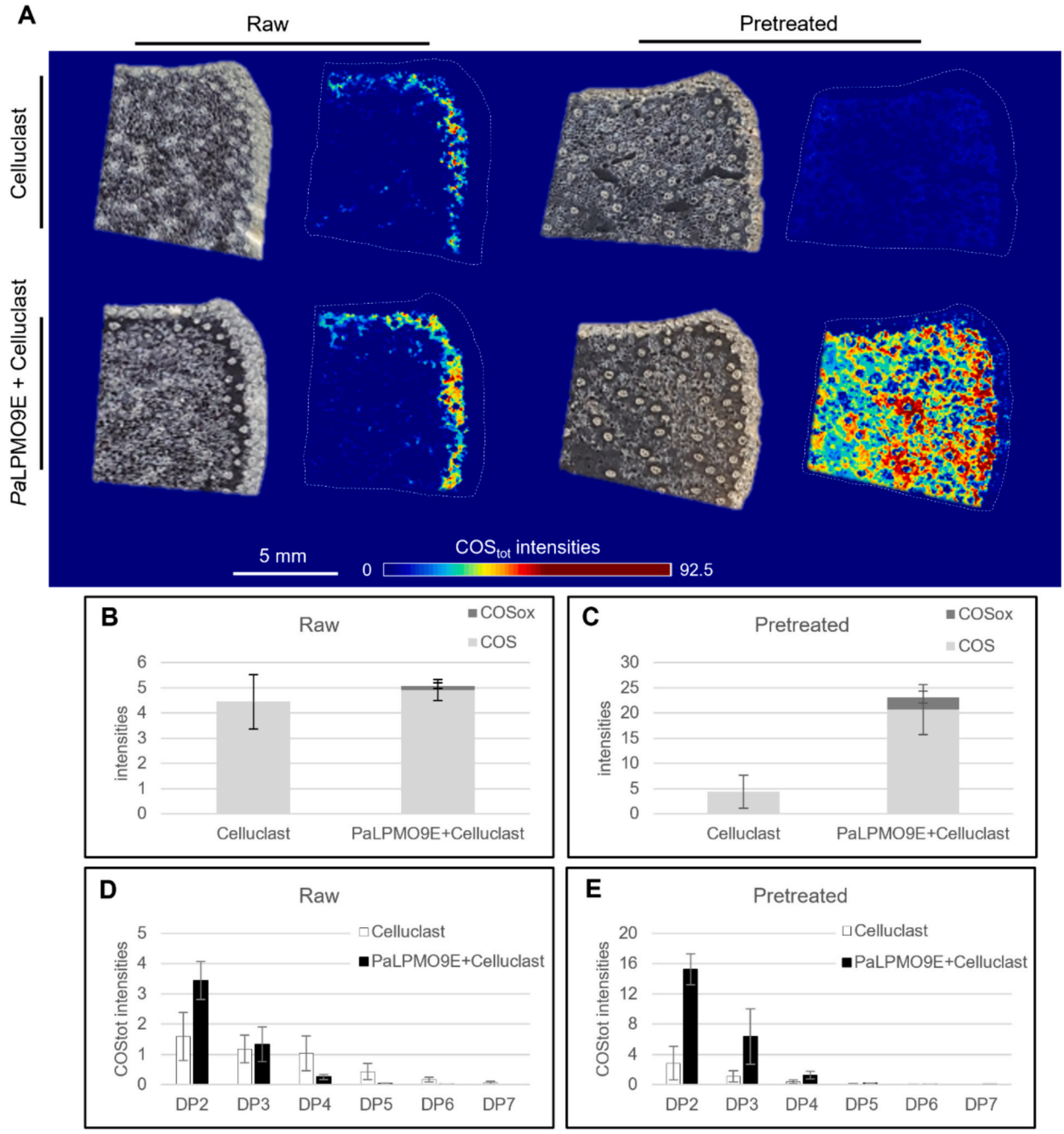

Fig. 2. Localisation and contribution to the MS signal of the total cello-oligosaccharides (COS_{tot}) released by the combined action of LPMO and Celluclast® (mass list of the species detected is in Table S1). (A) Light and MS images of raw and pretreated maize internode sections after enzyme application. MS images show the sum of the intensities of COS_{tot} species, both oxidised cello-oligosaccharides (COS_{ox}) and non-oxidised cello-oligosaccharides (COS). The colour scale runs from blue to red: red pixels correspond to the highest intensities, while dark blue pixels correspond to the lowest intensities. The dotted lines correspond to the area analysed. Square raster was set at 20 μm^2. (B) and (C) Contribution of COS_{ox} (dark grey) and COS (light grey) to the MS signal. (D) and (E) Contribution of COStot (according to degrees of polymerisation (DP), after hydrolysis by Celluclast® alone (white bar) or by LPMO + Celluclast® (black bar). Intensity values were collected from the mean MS spectra of each section. Values for (B), (C), (D) and (E) correspond to the average values obtained from four replicates of the MS imaging experiment: Fig. 2A, Supplementary material Figs. S3–S5 and Tables S2–S3).

confirms that the LPMO improves the performance of cellulases in the pretreated internode sections.

To characterise in-depth the in situ direct action of the LPMO, the contribution of each COS_{tot} with a degree of polymerisation (DP) between DP2 and DP7 to the total intensity was determined (Fig. 2D, E). Different profiles were observed depending on the action of the LPMO and the application of the pretreatment on maize sample. In the raw sample incubated with Celluclast® alone (Fig. 2D), a wide range of COS_{tot} was detected (from DP2 to DP7) with DP2, DP3 and DP4 being the most abundant species detected with similar intensities. In the raw sample, the addition of the LPMO impacted the relative distribution of COS (less DP4 and more DP2). In contrast, in the pretreated samples (Fig. 2E), the addition of the LPMO did not change the relative distribution of COS.

3.3. Mapping of the direct action of LPMO through the distribution of cellulose oxidised products

To investigate the effect of LPMO at the tissue level, we reconstructed images corresponding to the sum of COS_{ox} intensities between DP2 and DP7 (Fig. 3A), extracting the intensities of each species (Fig. 3B, C). Four replicates were performed for each condition (Figs. S7–S9). When Celluclast® alone was added to tissue sections, no COS_{ox} were detected in both raw and pretreated samples, confirming the negligible LPMO activity in this cocktail (Fig. 3A, B, C). When *Pa*LPMO9E was used alone, COS_{ox} were barely detected on raw sections (Fig. 3A, white arrow). In contrast, modifications induced by HWP clearly favoured the action of *Pa*LPMO9E with the release of significant amount of COS_{ox}. These COS_{ox}, mainly DP2 (Fig. 3C), were detected in abundance in the parenchyma under the rind and the parenchyma close to vascular bundles, and to a lower extent in the pith parenchyma (Fig. 3A).

In the raw sample, a significant increase of COS_{ox} release was observed in the parenchyma under the rind when the LPMO action was followed by incubation with Celluclast (Fig. 3A, white arrow). While the increase was even more striking in the pretreated internode, the amount of COS_{ox} detected appeared slightly lower than that observed when *Pa*LPMO9E was applied alone (Fig. 3C). These results suggest that for the raw samples, the action of cellulases is necessary to release COS_{ox} but their abundance remains at a low level. In the pretreated samples, the LPMO released COS_{ox} without the action of cellulases. The lower intensity of COS_{ox} observed when combining *Pa*LPMO9E with Celluclast® could either be due to the reduced incubation time when *Pa*LPMO9E was applied upstream (6 h versus 21 h when LPMO was used alone) or to the lack of detection of monosaccharides.

4. Discussion

Visualization of the direct effect of LPMO on plant cell wall polysaccharides has been the focus of intensive research efforts over the last few years. One of the main attempts was to get insights into LPMO binding at the cellulose surface. However, in most reports, the substrates used were cellulose microfibrils or nanocrystals, which do not take into account the complex structure of plant cell walls (Chemin et al., 2023;

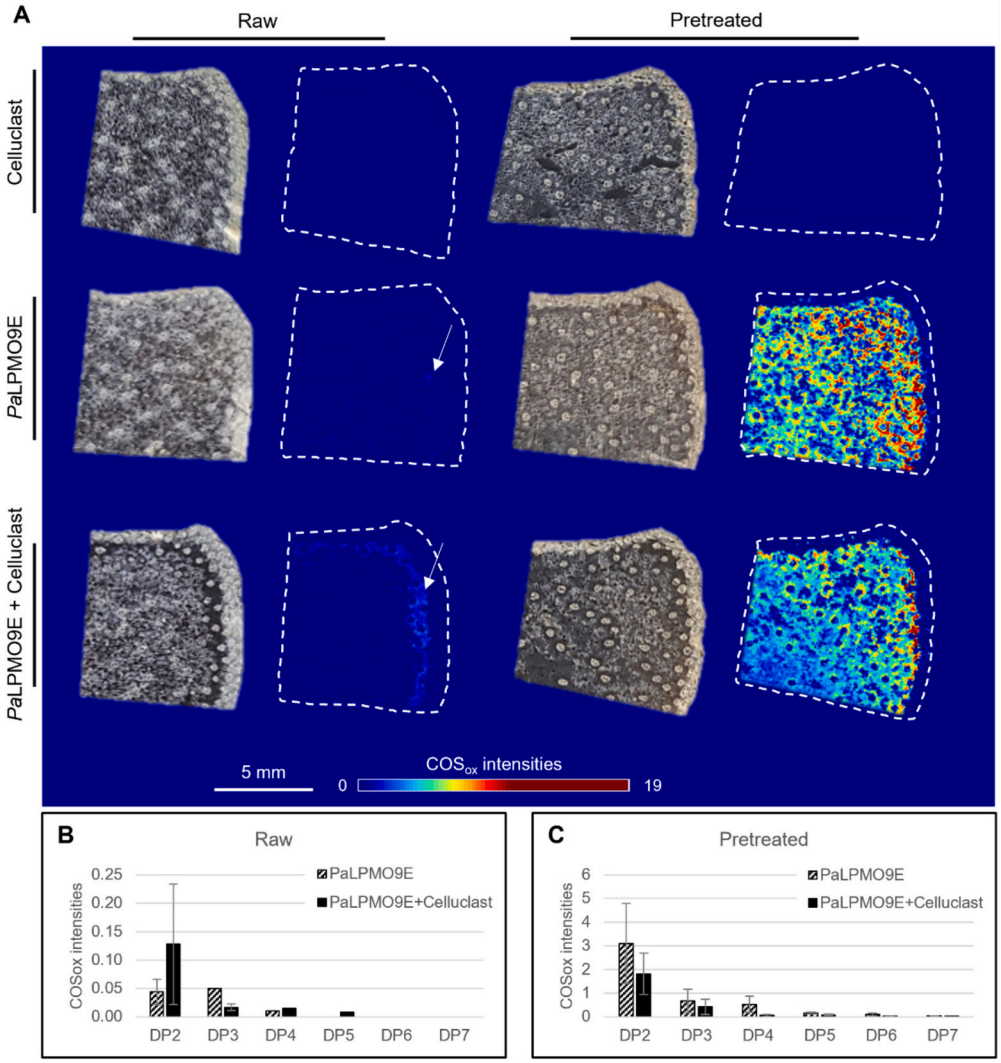

Fig. 3. Localisation and contribution to the MS signal of the COS_{ox} released by the action of LPMO ® (mass list of the species detected is in Table S1). (A) Light and MS images of raw and pretreated maize internode sections after enzyme application. MS images show the sum of the intensities of all COS_{ox} species. The colour scale runs from blue to red: red pixels correspond to the highest intensities while dark blue pixels correspond to the lowest intensities. The dotted lines correspond to the area analysed. Square raster was set at 20 μm^2. (B) and (C) Contribution to the MS signal of COS_{ox} according to the DP, after hydrolysis by LPMO alone (hatched white bar) or by LPMO + Celluclast® (black bar), no oxidised species were detected after hydrolysis by Celluclast® alone. Values for (B) and (C) correspond to the average values obtained from four replicates of the MS imaging experiment: Fig. 3A, Supplementary material Figs. S7–S9 and Tables S2–S3).

Eibinger et al., 2017; Uchiyama et al., 2022; Villares et al., 2017). Indeed, the intricacy of the cell wall affects the accessibility of the enzymes to their substrate as well as the activities of the enzymes themselves. Chabbert et al. (Chabbert et al., 2017) and Chang et al. (Chang et al., 2022) localised LPMOs in plant tissue sections using the autofluorescent properties of the proteins under deep UV excitation or by labelling the enzyme with a fluorophore. In situ activity and synergy with cellulolytic enzymes were demonstrated either by determining changes in cell wall composition monitored by FT-IR microspectroscopy, or by measuring the concentration of H_2O_2 in the vicinity of bound LPMO and glucose release using a piezometer-controlled H_2O_2 and glucose microsensor (Chabbert et al., 2017; Chang et al., 2022). Here, we localised and visualised LPMO activity by direct detection of COS_{ox} using MALDI MS imaging. Several features of MALDI MS imaging make it particularly interesting in this context. MALDI MS images can be used to map the distribution of products resulting from the action of enzymes on a representative surface of the sample with a resolution of a few µm without any labelling or specific probes. The distribution map of COS and COS_{ox} thus provides a direct indication of the local synergy between the enzymes.

MS imaging of LPMO action on plant tissues was challenging to develop (Fig. 1). Indeed, both *Pa*LPMO9E and cellulases have an affinity for cellulose and can compete for binding. Moreover, COS_{ox} are minor species when LPMOs are used in combination with cellulases. To overcome these limitations, the LPMO and Celluclast® were applied sequentially and the LPMO to Celluclast® ratio was modified while the incubation temperature was lowered. By applying this approach, for the first time, the direct action of an LPMO, via the release of oxidised compounds, could be localised and investigated at the tissue scale. In the raw samples, COS_{tot} were detected mainly in non-lignified tissues, in the parenchyma under the rind and, to a lesser extent, in the parenchyma surrounding the bundles. Adding the LPMO step before degradation by Celluclast® only moderately increased the quantity of COS_{tot} detected in the raw parenchyma under the rind and around bundles (Fig. 2A). One possible explanation is that the presence of hemicelluloses limits the LPMO access to cellulose and therefore its action (Arnaud et al., 2020; Devaux et al., 2018; Leroy et al., 2022). Xylan is the dominant hemicellulose in the cell walls of grasses. It consists in β-(1–4) linked xylosyl residues which can be decorated by sugar side chains and acetyl groups (Chandrakanth et al., 2023; Hatfield et al., 2017; Tryfona et al., 2023). The most abundant substituent is arabinose, which can be esterified by hydroxycinnamic acids, ferulic and *p*-coumaric acid (Hatfield et al., 2017). The substitution pattern and feruloylation of xylans have been shown to influence the way xylan interacts with cellulose and lignin (Gupta et al., 2023; Tryfona et al., 2023). Ferulate allows cross-linking xylan to other xylan chains and lignin by radical coupling, which contributes to the tight entanglement of cell wall polymers and may limit the diffusion of LPMO into the cell wall. It has also been shown that arabinoxylan populations with a uniform distribution of arabinose along the backbone can bind to the surface of cellulose fibrils (Tryfona et al., 2023), which could block LPMO action.

In pretreated samples, the partial removal of hemicelluloses and ferulic acid favoured the access of the LPMO to cellulose. As a result, oxidised species were detected in the non-lignified tissues throughout the entire section (Fig. 3A). This also resulted in a faster degradation of the cellulose, as evidenced by the release of a higher proportion of low DP COS_{tot} when Celluclast® was combined with LPMO compared to Celluclast® alone (Fig. 2E). In lignified tissues of the raw internodes (Fig. S6), whether LPMO was used alone or combined with Celluclast®, no COS_{tot} were detected (Fig. 2A). This probably comes from the effect of lignin, which is recognised as the main obstacle to enzymatic deconstruction, due to its amorphous structure and its ability to form inter-polymer bonds with hemicelluloses surrounding cellulose microfibrils, thus limiting cellulose accessibility to enzymes (Bichot et al., 2018; Chandra et al., 2007; Zoghlami & Paës, 2019). Moreover, lignin can compete with cellulose through non-specific and non-productive adsorption of enzymes (Yang & Pan, 2016), decreasing their availability for catalysis. In the pretreated samples, COS_{ox} (Fig. 3A) and COS (Fig. 2A) were detected in regions that were initially recalcitrant to enzyme degradation. Even if the chosen HWP only slightly affects lignin (Leroy et al., 2021), the partial loss of hemicelluloses and the modification of the lignin organisation both likely increase cell wall porosity, as demonstrated for other biomass samples (Herbaut et al., 2018). These modifications enable LPMO, as well as cellulases, to access and degrade cellulose.

5. Conclusions

In conclusion, the MALDI-MS imaging approach developed in this study allowed to follow direct action of an LPMO and revealed synergism with cellulases, at the tissue level. Maps of the distribution of oxidised and non-oxidised oligosaccharides released by the enzymes in a representative region of stem maize sections were obtained with a resolution of 20 µm. This showed that the interplay between LPMO and cellulases is affected by the structural characteristics of the cell wall, which vary from one tissue to another. In particular, the presence of lignin and hemicelluloses limit the access of LPMO to cellulose. The 40-min HWP removes these barriers by causing a partial loss of hemicelluloses and structural re-organisation of the lignin. MALDI-MS imaging has emerged a few years ago as a powerful method to study plant cell wall architectures and enzymes' activities on those architectures (Arnaud et al., 2020; Fanuel et al., 2018; Granborg et al., 2023; Leroy et al., 2022; Veličković et al., 2014). The method opens up opportunities to correlate multiscale chemical and structural changes at the polymer and tissue levels with enzyme efficiency. The present work provides a further illustration in that direction, as the method allowed to study the synergistic effects of various GHs and oxidases on cell wall degradation, taking into account the variability of cell wall properties in plant tissues. The results provide relevant directions to improve enzyme cocktails for biotechnological applications related to plant cell wall deconstruction.

Funding

This work was supported by Amandine Leroy's PhD fellowship funded by the Grand Est Region and the Grand Reims.

CRediT authorship contribution statement

Amandine Leroy: Writing – review & editing, Writing – original draft, Visualization, Validation, Methodology, Investigation, Formal analysis, Conceptualization. **Mathieu Fanuel:** Writing – review & editing, Writing – original draft, Visualization, Validation, Methodology, Investigation, Formal analysis, Conceptualization. **Camille Alvarado:** Writing – review & editing, Validation, Investigation. **Hélène Rogniaux:** Writing – review & editing, Writing – original draft, Validation, Methodology, Investigation, Conceptualization. **Sacha Grisel:** Writing – review & editing, Resources. **Mireille Haon:** Writing – review & editing, Resources. **Jean-Guy Berrin:** Writing – review & editing, Writing – original draft, Validation, Supervision, Resources, Investigation, Conceptualization. **Gabriel Paës:** Writing – review & editing, Writing – original draft, Validation, Supervision, Investigation, Conceptualization. **Fabienne Guillon:** Writing – review & editing, Writing – original draft, Validation, Supervision, Investigation, Conceptualization.

Declaration of competing interest

The authors declare that they have no known competing financial interests or personal relationships that could have appeared to influence the work reported in this paper.

Data availability

Data will be made available on request.

Acknowledgements

We thank Valérie Méchin (IJPB, INRAE, AgroParisTech, CNRS, Université Paris-Saclay, Versailles) for providing the maize plant samples.

Appendix A. Supplementary data

Supplementary data to this article can be found online at https://doi.org/10.1016/j.carbpol.2024.122465.

References

Agrawal, D., Basotra, N., Balan, V., Tsang, A., & Chadha, B. S. (2020). Discovery and expression of thermostable LPMOs from thermophilic fungi for producing efficient lignocellulolytic enzyme cocktails. *Applied Biochemistry and Biotechnology, 191*(2), 463–481. https://doi.org/10.1007/s12010-019-03198-5

Arnaud, B., Durand, S., Fanuel, M., Guillon, F., Méchin, V., & Rogniaux, H. (2020). Imaging study by mass spectrometry of the spatial variation of cellulose and hemicellulose structures in corn stalks. *Journal of Agricultural and Food Chemistry, 68*(13), 4042–4050. https://doi.org/10.1021/acs.jafc.9b07579

Bennati-Granier, C., Garajova, S., Champion, C., Grisel, S., Haon, M., Zhou, S., … Berrin, J.-G. (2015). Substrate specificity and regioselectivity of fungal AA9 lytic polysaccharide monooxygenases secreted by Podospora anserina. *Biotechnology for Biofuels, 8*(1), 90. https://doi.org/10.1186/s13068-015-0274-3

Bernardi, A. V., Gerolamo, L. E., de Gouvêa, P. F., Yonamine, D. K., Pereira, L. M. S., de Oliveira, A. H. C., … Dinamarco, T. M. (2020). LPMO AfAA9_B and cellobiohydrolase AfCel6A from a. fumigatus boost enzymatic saccharification activity of cellulase cocktail. *International Journal of Molecular Sciences, 22*(1). https://doi.org/10.3390/ijms22010276

Bichot, A., Delgenès, J.-P., Méchin, V., Carrère, H., Bernet, N., & García-Bernet, D. (2018). Understanding biomass recalcitrance in grasses for their efficient utilization as biorefinery feedstock. *Reviews in Environmental Science and Bio/Technology, 17*(4), 707–748. https://doi.org/10.1007/s11157-018-9485-y

Caputo, F., Tolgo, M., Naidjonoka, P., Krogh, K., Novy, V., & Olsson, L. (2023). Investigating the role of AA9 LPMOs in enzymatic hydrolysis of differentially steam-pretreated spruce. *Biotechnology for Biofuels and Bioproducts, 16*(1), 68. https://doi.org/10.1186/s13068-023-02316-0

Chabbert, B., Habrant, A., Herbaut, M., Foulon, L., Aguié-Béghin, V., Garajova, S., … Paës, G. (2017). Action of lytic polysaccharide monooxygenase on plant tissue is governed by cellular type. *Scientific Reports, 7*(1), 17792. https://doi.org/10.1038/s41598-017-17938-2

Chandra, R., Bura, R., Mabee, W., Berlin, A., Pan, X., & Saddler, J. (2007). Substrate pretreatment: The key to effective enzymatic hydrolysis of lignocellulosics? *Advances in Biochemical Engineering/Biotechnology, 108*, 67–93. https://doi.org/10.1007/10_2007_064

Chandrakanth, N. N., Zhang, C., Freeman, J., de Souza, W. R., Bartley, L. E., & Mitchell, R. A. C. (2023). Modification of plant cell walls with hydroxycinnamic acids by BAHD acyltransferases. *Frontiers in Plant Science, 13*. https://doi.org/10.3389/fpls.2022.1088879

Chang, H., Gacias Amengual, N., Botz, A., Schwaiger, L., Kracher, D., Scheiblbrandner, S., … Ludwig, R. (2022). Investigating lytic polysaccharide monooxygenase-assisted wood cell wall degradation with microsensors. *Nature Communications, 13*(1), 6258. https://doi.org/10.1038/s41467-022-33963-w

Chemin, M., Kansou, K., Cahier, K., Grellier, M., Grisel, S., Novales, B., … Cathala, B. (2023). Optimized lytic polysaccharide monooxygenase action increases fiber accessibility and fibrillation by releasing tension stress in cellulose cotton fibers. *Biomacromolecules, 24*(7), 3246–3255. https://doi.org/10.1021/acs.biomac.3c00303

Devaux, M. F., Jamme, F., Andre, W., Bouchet, B., Alvarado, C., Durand, S., … Guillon, F. (2018). Synchrotron time-lapse imaging of lignocellulosic biomass hydrolysis: Tracking enzyme localization by protein autofluorescence and biochemical modification of cell walls by microfluidic infrared microspectroscopy. *Frontiers in Plant Science, 9*, 200. https://doi.org/10.3389/fpls.2018.00200

Eibinger, M., Ganner, T., Bubner, P., Rosker, S., Kracher, D., Haltrich, D., … Nidetzky, B. (2014). Cellulose surface degradation by a lytic polysaccharide monooxygenase and its effect on cellulase hydrolytic efficiency. *The Journal of Biological Chemistry*. https://doi.org/10.1074/jbc.M114.602227

Eibinger, M., Sattelkow, J., Ganner, T., Plank, H., & Nidetzky, B. (2017). Single-molecule study of oxidative enzymatic deconstruction of cellulose. *Nature Communications, 8*(1), 894. https://doi.org/10.1038/s41467-017-01028-y

Fanuel, M., Ropartz, D., Guillon, F., Saulnier, L., & Rogniaux, H. (2018). Distribution of cell wall hemicelluloses in the wheat grain endosperm: A 3D perspective. *Planta, 248*. https://doi.org/10.1007/s00425-018-2980-0

Frandsen, K., Haon, M., Grisel, S., Henrissat, B., Lo Leggio, L., & Berrin, J.-G. (2020). Identification of the molecular determinants driving the substrate specificity of fungal lytic polysaccharide monooxygenases (LPMOs). *Journal of Biological Chemistry, 296*. https://doi.org/10.1074/jbc.RA120.015545

Frommhagen, M., Mutte, S. K., Westphal, A. H., Koetsier, M. J., Hinz, S. W. A., Visser, J., … Kabel, M. A. (2017). Boosting LPMO-driven lignocellulose degradation by polyphenol oxidase-activated lignin building blocks. *Biotechnology for Biofuels, 10*, 121. https://doi.org/10.1186/s13068-017-0810-4

Granborg, J. R., Kaasgaard, S. G., & Janfelt, C. (2023). Variation in oligosaccharide profiles observed with AP-MALDI in different regions of maize kernels after treatment with xylanases. *Journal of Cereal Science, 109*, Article 103586. https://doi.org/10.1016/j.jcs.2022.103586

Grieco, M. A. B., Haon, M., Grisel, S., de Oliveira-Carvalho, A. L., Magalhães, A. V., Zingali, R. B., … Berrin, J.-G. (2020). Evaluation of the enzymatic arsenal secreted by Myceliophthora thermophila during growth on sugarcane bagasse with a focus on LPMOs. *Frontiers in Bioengineering and Biotechnology, 8*(1028). https://doi.org/10.3389/fbioe.2020.01028

Gupta, M., Dupree, P., Petridis, L., & Smith, J. C. (2023). Patterns in interactions of variably acetylated xylans with hydrophobic cellulose surfaces. *Cellulose, 30*(18), 11323–11340. https://doi.org/10.1007/s10570-023-05584-z

Gupta, V. K., Kubicek, C. P., Berrin, J.-G., Wilson, D. W., Couturier, M., Berlin, A., … Ezeji, T. (2016). Fungal enzymes for bio-products from sustainable and waste biomass. *Trends in Biochemical Sciences, 41*(7), 633–645. https://doi.org/10.1016/j.tibs.2016.04.006

Harris, P. V., Welner, D., McFarland, K. C., Re, E., Navarro Poulsen, J.-C., Brown, K., … Lo Leggio, L. (2010). Stimulation of lignocellulosic biomass hydrolysis by proteins of glycoside hydrolase family 61: Structure and function of a large, enigmatic family. *Biochemistry, 49*(15), 3305–3316. https://doi.org/10.1021/bi100009p

Hatfield, R. D., Rancour, D. M., & Marita, J. M. (2017). Grass cell walls: A story of cross-linking. *Frontiers in Plant Science, 7*(2056). https://doi.org/10.3389/fpls.2016.02056

Herbaut, M., Zoghlami, A., Habrant, A., Falourd, X., Foucat, L., Chabbert, B., & Paës, G. (2018). Multimodal analysis of pretreated biomass species highlights generic markers of lignocellulose recalcitrance. *Biotechnology for Biofuels, 11*, 52. https://doi.org/10.1186/s13068-018-1053-8

Leroy, A., Devaux, M.-F., Fanuel, M., Chauvet, H., Durand, S., Alvarado, C., … Guillon, F. (2022). Real-time imaging of enzymatic degradation of pretreated maize internodes reveals different cell types have different profiles. *Bioresource Technology, 353*, Article 127140. https://doi.org/10.1016/j.biortech.2022.127140

Leroy, A., Falourd, X., Foucat, L., Méchin, V., Guillon, F., & Paës, G. (2021). Evaluating polymer interplay after hot water pretreatment to investigate maize stem internode recalcitrance. *Biotechnology for Biofuels, 14*(1), 164. https://doi.org/10.1186/s13068-021-02015-8

Long, L., Yang, H., Ren, H., Liu, R., Sun, F. F., Xiao, Z., … Xu, Z. (2020). Synergism of recombinant Podospora anserina PaAA9B with cellulases containing AA9s can boost the enzymatic hydrolysis of cellulosic substrates. *ACS Sustainable Chemistry & Engineering, 8*(32), 11986–11993. https://doi.org/10.1021/acssuschemeng.0c02564

Moon, M., Lee, J.-P., Park, G. W., Lee, J.-S., Park, H. J., & Min, K. (2022). Lytic polysaccharide monooxygenase (LPMO)-derived saccharification of lignocellulosic biomass. *Bioresource Technology, 359*, Article 127501. https://doi.org/10.1016/j.biortech.2022.127501

Munzone, A., Eijsink, V. G. H., Berrin, J.-G., & Bissaro, B. (2024). Expanding the catalytic landscape of metalloenzymes with lytic polysaccharide monooxygenases. *Nature Reviews Chemistry*. https://doi.org/10.1038/s41570-023-00565-z

Pu, Y., Hu, F., Huang, F., Davison, B. H., & Ragauskas, A. J. (2013). Assessing the molecular structure basis for biomass recalcitrance during dilute acid and hydrothermal pretreatments. *Biotechnology for Biofuels, 6*(1), 15. https://doi.org/10.1186/1754-6834-6-15

Ropartz, D., Bodet, P.-E., Przybylski, C., Gonnet, F., Daniel, R., Fer, M., … Rogniaux, H. (2011). Performance evaluation on a wide set of matrix-assisted laser desorption ionization matrices for the detection of oligosaccharides in a high-throughput mass spectrometric screening of carbohydrate depolymerizing enzymes. *Rapid Communications in Mass Spectrometry, 25*(14), 2059–2070. https://doi.org/10.1002/rcm.5060

Sagarika, M. S., Parameswaran, C., Senapati, A., Barala, J., Mitra, D., Prabhukarthikeyan, S. R., … Panneerselvam, P. (2022). Lytic polysaccharide monooxygenases (LPMOs) producing microbes: A novel approach for rapid recycling of agricultural wastes. *Science of the Total Environment, 806*, Article 150451. https://doi.org/10.1016/j.scitotenv.2021.150451

Tandrup, T., Frandsen, K. E. H., Johansen, K. S., Berrin, J. G., & Lo Leggio, L. (2018). Recent insights into lytic polysaccharide monooxygenases (LPMOs). *Biochemical Society Transactions, 46*(6), 1431–1447. https://doi.org/10.1042/bst20170549

Tokin, R., Ipsen, J.Ø., Westh, P., & Johansen, K. S. (2020). The synergy between LPMOs and cellulases in enzymatic saccharification of cellulose is both enzyme- and substrate-dependent. *Biotechnology Letters, 42*(10), 1975–1984. https://doi.org/10.1007/s10529-020-02922-0

Tryfona, T., Bourdon, M., Delgado Marques, R., Busse-Wicher, M., Vilaplana, F., Stott, K., & Dupree, P. (2023). Grass xylan structural variation suggests functional specialization and distinctive interaction with cellulose and lignin. *The Plant Journal, 113*(5), 1004–1020. https://doi.org/10.1111/tpj.16096

Uchiyama, T., Uchihashi, T., Ishida, T., Nakamura, A., Vermaas, J. V., Crowley, M. F., … Igarashi, K. (2022). Lytic polysaccharide monooxygenase increases cellobiohydrolases activity by promoting decrystallization of cellulose surface. *Science Advances, 8*(51), eade5155. https://doi.org/10.1126/sciadv.ade5155

Vandhana, T. M., Reyre, J.-L., Sushmaa, D., Berrin, J.-G., Bissaro, B., & Madhuprakash, J. (2022). On the expansion of biological functions of lytic polysaccharide monooxygenases. *New Phytologist, 233*(6), 2380–2396. https://doi.org/10.1111/nph.17921

Veličković, D., Ropartz, D., Guillon, F., Saulnier, L., & Rogniaux, H. (2014). New insights into the structural and spatial variability of cell-wall polysaccharides during wheat grain development, as revealed through MALDI mass spectrometry imaging. *Journal of Experimental Botany, 65*(8), 2079–2091. https://doi.org/10.1093/jxb/eru065

Vermaas, J. V., Crowley, M. F., Beckham, G. T., & Payne, C. M. (2015). Effects of lytic polysaccharide monooxygenase oxidation on cellulose structure and binding of oxidized cellulose oligomers to cellulases. *The Journal of Physical Chemistry B, 119* (20), 6129–6143. https://doi.org/10.1021/acs.jpcb.5b00778

Villares, A., Moreau, C., Bennati-Granier, C., Garajova, S., Foucat, L., Falourd, X., … Cathala, B. (2017). Lytic polysaccharide monooxygenases disrupt the cellulose fibers structure. *Scientific Reports, 7*(1), 40262. https://doi.org/10.1038/srep40262

Westereng, B., Cannella, D., Agger, J., Jørgensen, H., Andersen, M., Eijsink, V., & Felby, C. (2015). Enzymatic cellulose oxidation is linked to lignin by long-range electron transfer. *Scientific Reports, 5*, 18561. https://doi.org/10.1038/srep18561

Yang, Q., & Pan, X. (2016). Correlation between lignin physicochemical properties and inhibition to enzymatic hydrolysis of cellulose. *Biotechnology and Bioengineering, 113* (6), 1213–1224. https://doi.org/10.1002/bit.25903

Zhou, X., Xu, Z., He, J., Li, Y., Pan, C., Wang, C., … Zhu, H. (2020). A myxobacterial LPMO10 has oxidizing cellulose activity for promoting biomass enzymatic saccharification of agricultural crop straws. *Bioresource Technology, 318*, Article 124217. https://doi.org/10.1016/j.biortech.2020.124217

Zoghlami, A., & Paës, G. (2019). Lignocellulosic biomass: Understanding recalcitrance and predicting hydrolysis. *Frontiers in Chemistry, 7*(874). https://doi.org/10.3389/fchem.2019.00874